Analysis of the Training Behavior of the MICE Spectrometer Solenoid

Holger Witte, Heng Pan, Andrew Marone, Soren Prestemon, and Alan Bross

Abstract—**Muon ionization cooling is theoretically well understood but has never been fully demonstrated experimentally. Ionization cooling is regarded as an important technology both in terms of cost and performance for a Neutrino Factory and is absolutely essential for a Muon Collider. The MICE experiment (Muon Ionization Cooling Experiment), based at the Rutherford Appleton Laboratory, U.K., is currently collecting data to prove the concept. Part of MICE are two spectrometer magnets, each consisting of five superconducting large bore solenoids. The spectrometer solenoid is designed for a peak field of 4T. Both spectrometer magnets required about 15 quenches to reach the design current. However, it was discovered that both spectrometers do not remember their training; after a warm-up the spectrometers have to be retrained, following a very similar training curve. The MICE spectrometer was analyzed using 2-D and 3-D finite element software to understand the quench and training behavior; the analysis revealed a clamping mechanism, leading to a stick-slip situation for one of the coils in its coil pocket. This paper summarizes the results and makes suggestions how to improve the design.**

Index Terms—**Accelerator magnet, finite-element analysis, stress, superconducting magnets.**

I. Introduction

MICE is a ~10 m long beamline which aims to demonstrate ionization cooling experimentally [1]. MICE consists of several large bore low temperature superconducting solenoids, which are installed at the Rutherford Appleton Laboratory in the UK. At the beginning and end of the MICE channel are tracker magnets, which are used to measure the emittance change of the muon beam [2]. Each tracker magnet consists of five superconducting solenoids: two matching coils (M1 and M2) match the beam into the tracker magnet. This is followed by a 1.3 m long solenoid (labelled centre coil), which is located in-between two shorter solenoids (end coils E1 and E2) to extend the good field region.

The solenoids are wound from the same NbTi superconductor with a Cu:Sc ratio of four. Each of the tracker magnets consists of a single coil bobbin with pockets for the solenoids. The coil bobbin is made of forged aluminium (Al-6061-T6). Aluminium was also chosen for the bobbin to utilize quench-back, which refers to the effect that the coils are inductively coupled to the aluminium former and therefore can quench faster [3]. The magnets are wet-wound with epoxy. Fig. 1 shows the geometry of a tracker magnet schematically.

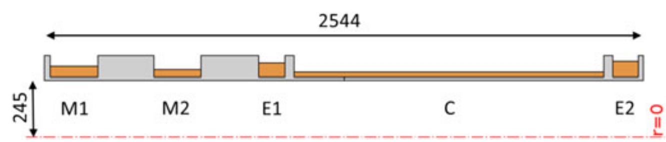

Fig. 1. Geometry of the MICE spectrometer solenoid. All dimensions in mm.

Both magnets during training showed a similar behaviour in that quenches occurred relatively early on (at about half of the operating current) and neither of the magnets ‘remembered’ its training. That means that after a thermal cycle both magnets have to be re-trained, following a very similar training curve. About 70% of the quenches originated in the E2 coil. Fig. 2 shows examples of typical training curves; as shown in the figure, the spectrometer magnets achieved the target training current of 283 A after 13 and 16 quenches.

When the first quench occurred all coils had about 70–80% margin on the load-line, so it seems unlikely that insufficient margin is the reason for the early coil quenches. Also, this would not explain the necessity to retrain the magnets after warm-up. This paper reports on the results of a finite element analysis, looking for mechanical reasons for this behaviour. The next section gives details about the analysis, which is followed by the simulation results.

II. Analysis Details

1) Geometry: Table I shows the coil dimensions used in the simulation, which have been taken from [4]. In the table r_i denotes the inner radius, dr the radial coil thickness, z_1 the longitudinal position (in the MICE reference system) and dz the coil length. J is the coil current density. For the analysis we use the dimensions for the upstream tracker (SSU). The inner radius of coil bobbin is 245 mm and the outer radius is 350 mm; the overall length of the coil bobbin is 2544 mm.

2) Material Properties: for the critical current density of NbTi we use the fit from Bottura [5]; for the thermal expansion coefficient we use $12.6 \times 10^{-6}\ \mathrm{K}^{-1}$. For the mechanical

Manuscript received August 23, 2017; accepted November 2, 2017. Date of publication November 13, 2017; date of current version November 30, 2017. This work was supported by Brookhaven Science Associates, LLC under Contract No. DE-SC0012704 with the U.S. Department of Energy. *(Corresponding author: Holger Witte.)*

H. Witte and A. Marone are with Brookhaven National Laboratory, Upton, NY 11973 USA (e-mail: hwitte@bnl.gov; andym@bnl.gov).

H. Pan and S. Prestemon are with Lawrence Berkeley National Laboratory, Berkeley, CA 94720 USA (e-mail: hengpan@lbl.gov; SOPrestemon@lbl.gov).

A. Bross is with Accelerator Physics Center, Fermilab, Batavia, IL 60510 USA (e-mail: bross@fnal.gov).

Color versions of one or more of the figures in this paper are available online at http://ieeexplore.ieee.org.

Digital Object Identifier 10.1109/TASC.2017.2772875

This manuscript has been authored by Fermi Research Alliance, LLC under Contract No. DE-AC02-07CH11359 with the U.S. Department of Energy, Office of Science, Office of High Energy Physics.

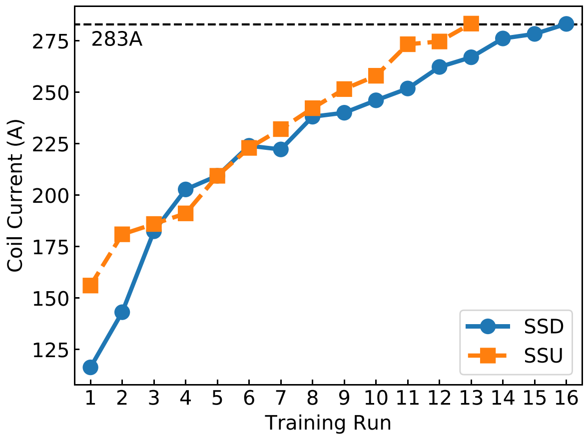

Fig. 2. Training history of the MICE spectrometer solenoids. SSD is the downstream tracker and SSU the upstream tracker.

TABLE I
MICE Coil Configuration

	r_i (m)	dr (m)	z_1 (m)	dz (m)	J (A/mm^2)
M1	0.258	0.0462	−3.7116	0.2012	118
M2	0.258	0.0309	−4.1508	0.1995	142
E1	0.258	0.0609	−5.8582	0.1106	149
SS	0.258	0.0221	−5.8582	1.3143	148
E2	0.258	0.0678	−6.0063	0.1106	148

analysis we use an orthotropic material model with properties from [6]. The bobbin is made of Al-6061 T6; we use a Young's modulus of 69 GPa and a Poission-ratio of 0.33. The coefficient of thermal expansion is 23.4×10^{-6} K^{-1}.

3) Simulation Details: for the simulations we use the commercial finite element software COMSOL[1]. The magnetic field is calculated in a 2D axisymmetric simulation; structural simulations are carried out in 2D axisymmetric or 3D simulations. The Lorentz force is applied to the structure in both cases via an extrusion coupling variable.

2D quasi-static and transient simulation were carried out; 3D simulations were limited to quasi-static simulations (it was found that the simulation time of 3D transient simulations is prohibitive when using contact elements). As a first step in each simulation pre-strain to the conductor is applied; we apply -0.1%, which is consistent with data from the winding sheets of the magnets. The structure is then assumed to be cooled down to 4K. Subsequently the electromagnetic force is applied. The various steps are implemented as load cases in COMSOL, using the solution of the previous load case as a starting point. Loads are usually applied in 10% steps.

The interface between the bobbin and the coils is modelled using contact elements. The exact properties of this interface are not known, but we assume a friction coefficient of 0.2; it was verified that smaller and larger values (between 0.05 and 0.3) of the friction coefficient do not affect the main conclusions of this

[1]COMSOL AB, Tegnérgatan 23, SE-111 40 Stockholm, Sweden.

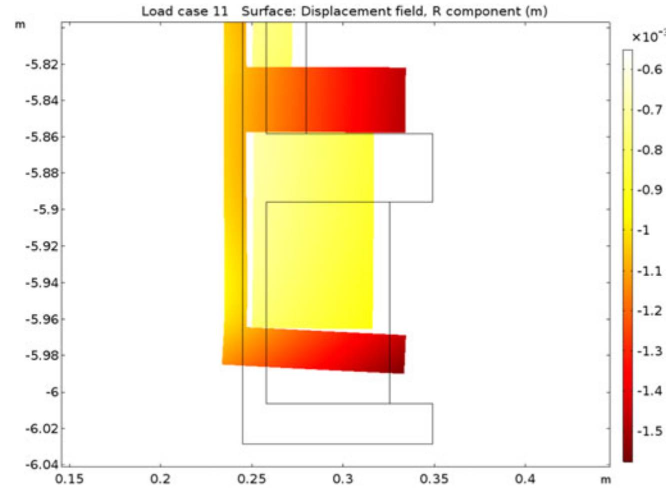

Fig. 3. Deformation plot of the E2 coil and the bobbin (deformation ten times amplified). The colour indicates the radial displacement.

study. For 2D static models we use the augmented Lagrangian method for the contact algorithm. To aid convergence a small contact pressure of a few MPa is applied to the interface. For 3D and time-dependent models we use the simpler but robuster penalty method. Plastic deformation is not considered.

III. Simulation Results

A. Initial Cool-Down

The simulations show that due to the different thermal expansion coefficients the superconducting magnet detaches from the coil bobbin and a gap in radial direction occurs. Each coil is held in place longitudinally by its aluminium support. The simulation results indicate an interesting behaviour for the E2 coil, which is shown in Fig. 3.

The figure shows that the lower flange in axial direction detaches from the coil E2; due to this partial detachment the coil is held less strongly in place than other coils. The M1 coil shows a similar behaviour, but the effect is less pronounced. The other coils did not show an opening of the coil pockets.

B. Electromagnetic Force

Subsequently the electromagnetic force was applied to the structure. Initially this was done in a quasi-static simulation; 25%, 40%, 60%, 80% and 100% of the electromagnetic force is applied in 10% steps using load cases. After each of these cycles the electromagnetic load was reduced to zero. The simulations show that in particular the E2 coil does not return to its original position (after cool-down), which suggests that the coil is slipping in its coil pocket.

This is shown in Fig. 4, which shows the radial displacement of the E2 coil (lower flange) for various load cycles. The figure shows that the radial displacement increases after each of the described load scenarios due to the Lorentz force. This behaviour was most pronounced for the E2 coil (by a factor two or more).

This can be explained by the forces acting on the E2 coil; like in any solenoid there is a large radial body force and a

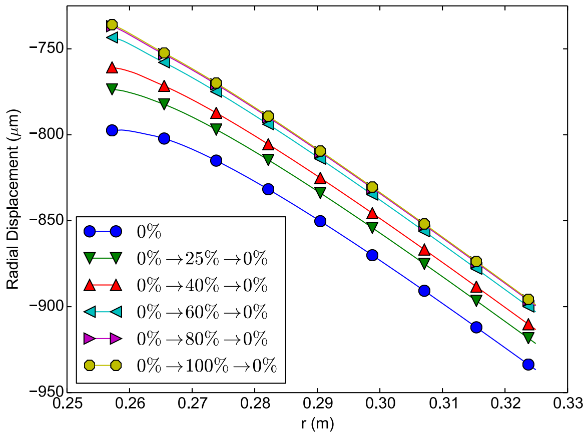

Fig. 4. Radial displacement of the lower E2 boundary for various mechanical load scenarios.

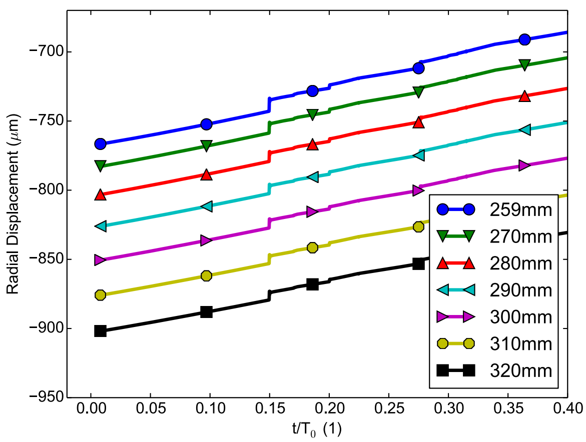

Fig. 5. Time dependent radial displacement of different points on the lower E2 boundary.

longitudinal force acting to compress the magnet axially. In addition, there is second force contribution in longitudinal direction from the interaction with the nearby centre coil. This interaction leads to a substantial additional longitudinal force (1.6 MN) which pulls the E2 magnet towards the centre coil, away from the partially detached flange. While there is also a net longitudinal force on the M1 coil, it is only about $1/4$ of this (400 kN).

Further detailed simulations concentrated on the behaviour of E2, which was studied in a time-dependent study. To keep the simulation times reasonable the rest of the aluminium bobbin and coils are not included. The upper boundary of the E2 coil pocket is defined as axially fixed; it was verified that the radial displacement of the E2 coil and pocket remains similar to what was observed for the full structure.

Fig. 5 shows the radial displacement of the lower coil-bobbin interface at several positions. At $t = \mathrm{T}_0$ the full electromagnetic force is applied (the time base is arbitrary, inertial effects are not considered). The simulation suggests that the movement at this interface cannot be expected to be smooth; at $t/\mathrm{T}_0 = 0.15$ and 0.275 jumps in the radial displacement can be observed, indicating a stick-slip behaviour.

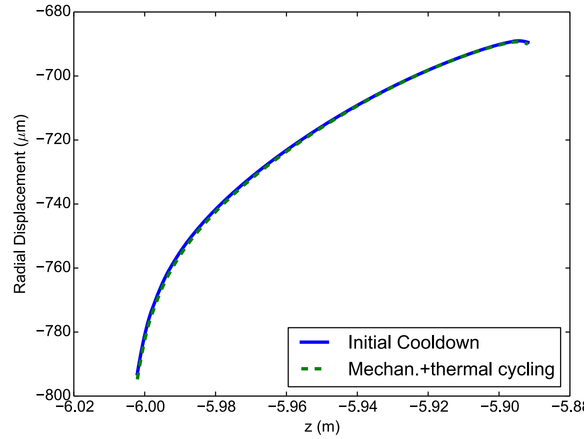

Fig. 6. Radial displacement of E2 (inner radius) for the initial cool-down and after mechanical and thermal cycling.

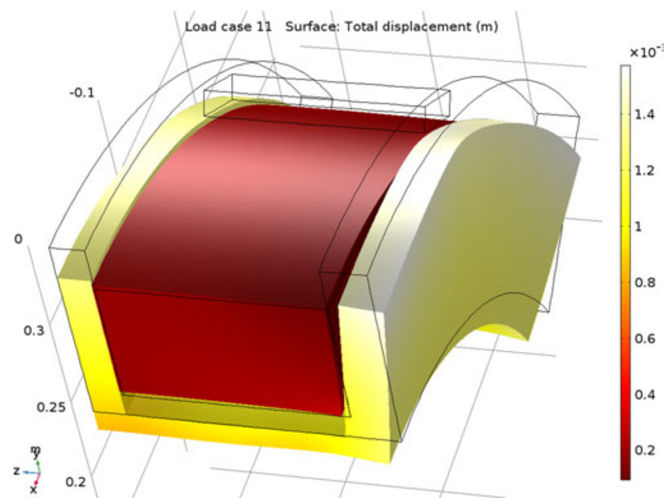

Fig. 7. Analysis of the thermal contraction of the E2 coil in its coil pocket with an axial support bar.

C. Thermal Cycling

To study the effect of thermal cycling a quasi-static simulation was employed. The simulation shows that a warm-up (after mechanical loading) allows the coils to return to their original position; a subsequent cool-down is indistinguishable from the initial cool-down. This is the case for all coils; Fig. 6 shows this for the E2 coil; the figure shows the radial displacement at the inner radius of the E2 coil for the initial cool-down and a second cool-down after mechanical and thermal cycling.

D. Axial Support - 3D Analysis

From pictures taken during coil construction it is known that axial support bars made of Al-6061-T6 are installed in the coil pockets to prevent the coil pockets from opening up. The exact dimensions are unknown; for the simulation we assume a cross-section of 0.5" $\times$ 1" [7]. For SSU six of these bars are installed.

Fig. 7 shows the deformation (amplified by factor 10) after cool-down. The colour indicates the total displacement. As shown in the figure, the axial support strut prevents partially the movement of the coil bobbin, but any effect is limited to its

TABLE II
OPTIMIZED MICE COIL CONFIGURATION

	r_i (m)	dr (m)	z_1 (m)	dz (m)	J (A/mm^2)
M1	0.258	0.0462	−3.7116	0.2012	142
M2	0.258	0.0309	−4.1508	0.1995	151
E1	0.258	0.0793	−4.518	0.11613	83.9
SS	0.258	0.022	−5.8536	1.3143	149.4
E2	0.258	0.0763	−6.0013	0.13272	93.19

TABLE III
OPERATING MARGINS

	Original	Optimized	Optimized/Step V'
E2	0.3	0.43	0.43
SS	0.44	0.43	0.44
E1	0.34	0.46	0.46
M2	0.43	0.435	0.589
M1	0.35	0.354	0.43

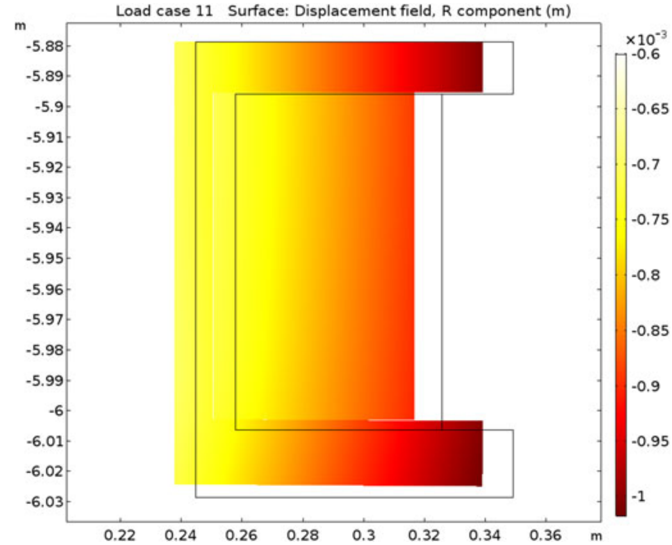

Fig. 8. The E2 coil pocket after cool-down. The colour indicates the radial displacement; the deformation is amplified by a factor of 10.

direct vicinity. Large parts of the bobbin still separate from the coil; it is therefore unlikely that the support struts are able to suppress the movement of the E2 coil in its pocket.

IV. DESIGN IMPROVEMENTS

To improve the behaviour of the MICE spectrometer solenoid several design changes can be thought of. The coil geometry can be optimized to increase the operating margin as shown in the next section; possible mechanical improvements will be discussed in the subsequent subsection.

A. *Optimized Geometry*

The coil geometry of the MICE spectrometer can be improved to increase the margins. This was evaluated with the Nelder-Mead optimization algorithm in COMSOL. In the simulation we allow the geometry of E1, E2 and SS to vary; the inner radii of the coils remain fixed at 258 mm. In the simulation the target criteria are the field quality in the centre solenoid over a length of 1 m (required to be better than 1%) while increasing the temperature margin. The optimized coil configuration is shown in table II.

In comparison to the original configuration E1 and E2 have increased in cross-section, which reduces the current densities by 30–35%. The operating margin in E2 increases to 43% on the load-line in testing conditions; the results are summarized in table III. For Step V' operation, which is one of the run modes of MICE, the operating margin is 43% or more.

B. *Mechanical Improvements*

The analysis revealed that the individual coils separate from the bobbin; this is caused by different thermal expansion coefficients of the materials. This can be avoided when using austenitic stainless steel for the bobbin, which possesses a similar thermal expansion coefficient to NbTi. This is shown in Fig. 8; no separation is observed between bobbin and coil. The figure also shows that the overall deformation of the bobbin is reduced.

Studies show that using stainless steel as a mandrel implies that quench-back does not occur, which has to be considered for quench protection of the magnet [8].

Coil movement during operation can be minimized by winding the conductor with sufficient wire pre-tension. Simulations show that a wire tension equivalent to 120 MPa is required to reduce coil movement to less than 100 μm. A stick-slip scenario is not observed in this case for the E2 coil. Other options of stress management are possible and should be explored for similar coil designs.

V. CONCLUSION

While some of the input parameters of the simulations are not well defined (for example the exact properties of the coil/bobbin interface), it is not very likely that the general trend seen in the simulations will change. The analysis shows that due to the different thermal expansion coefficients the bobbin shrinks at a different rate than the superconducting magnets during cool-down. This leads to the coils separating from the coil bobbin; the coils are held longitudinally by the aluminium flanges. For the E2 and M1 coil the end flanges partially detach from the coils.

The simulations show that due to the electromagnetic force it is possible that at least the E2 coil can slip in its coil pocket. A time-dependent simulation suggests that it is likely that this will lead to a stick-slip situation, which dissipates heat and can lead to quenching. The M1 coil may be less prone to this as the net longitudinal force is smaller by a factor of four. Thermal cycling of the spectrometer solenoid allows the coils to return to their original position; a subsequent cool-down and energizing of the coils should therefore lead to a similar behaviour, which is consistent with the observed training behaviour.

References

[1] M. Bogomilov *et al.*, “The MICE Muon Beam on ISIS and the beam-line instrumentation of the muon ionization cooling experiment,” *J. Instrum.*, vol. 7, no. 05, May 2012, Art. no. P05009. [Online]. Available: http://stacks.iop.org/1748–0221/7/i=05/a=P05009 http://stacks.iop.org/1748–0221/7/i=05/a=P05009?key=crossref.80ab143932a9bbb1cb77ddc44e45f39b

[2] B. Wang *et al.*, “The design and construction of the MICE spectrometer solenoids,” *IEEE Trans. Appl. Supercond.*, vol. 19, no. 3, pp. 1348–1351, Jun. 2009.

[3] M. Green, “The development of large high current density superconducting solenoid magnets for use in high energy physics experiments,” Ph.D. dissertation, Lawrence Berkeley Lab., Univ. of California, Berkeley, CA, USA, May 1977.

[4] V. Blackmore and J. Tarrant, “As-built solenoid coil dimensions and locations in MICE Step IV,” MICE Note 464, Tech. Rep., 2015. [Online]. Available: http://mice.iit.edu/micenotes/public/pdf/MICE0464 /MICE0464.pdf

[5] L. Bottura, “A practical fit for the critical surface of NbTi,” *IEEE Trans. Appl. Supercond.*, vol. 10, no. 1, pp. 1054–1057, Mar. 2000. [Online]. Available: http://ieeexplore.ieee.org/lpdocs/epic03/wrapper.htm?arnumber=828413

[6] I. Dixon, R. Walsh, W. Markiewicz, and C. Swenson, “Mechanical properties of epoxy impregnated superconducting solenoids,” *IEEE Trans. Magn.*, vol. 32, no. 4, pp. 2917–2920, Jul. 1996. [Online]. Available: http://ieeexplore.ieee.org/lpdocs/epic03/wrapper.htm?arnumber=511486

[7] S. Virostek, private communication, Lawrence Berkeley Nat. Lab., Berkeley, CA, USA.

[8] X. L. Guo, M. A. Green, L. Wang, H. Pan, and H. Wu, “The role of quench-back in the passive quench protection of long solenoids with coil sub-division,” *IEEE Trans. Appl. Supercond.*, vol. 20, no. 3, pp. 2035–2038, Jun. 2010.